Journal of Controlled Release 239 (2016) 149–158

Contents lists available at ScienceDirect

Journal of Controlled Release

journal homepage: www.elsevier.com/locate/jconrel

# Robust, tumor-homing and redox-sensitive polymersomal doxorubicin: A superior alternative to Doxil and Caelyx?

Yan Zou, Fenghua Meng *, Chao Deng, Zhiyuan Zhong *

*Biomedical Polymers Laboratory, Jiangsu Key Laboratory of Advanced Functional Polymer Design and Application, College of Chemistry, Chemical Engineering and Materials Science, Soochow University, Suzhou 215123, PR China*

ARTICLE INFO

*Article history:*
Received 1 June 2016
Received in revised form 18 August 2016
Accepted 21 August 2016
Available online 25 August 2016

*Keywords:*
Polymersomes
Lung cancer
Drug delivery
Reduction-sensitive
Targeted delivery
Chemotherapy

ABSTRACT

Pegylated liposomal doxorubicin (Lipo-Dox) is one of the few clinically used cancer nanomedicines. Here we show that tumor-homing, redox-responsive and reversibly crosslinked multifunctional biodegradable polymersomes are a better alternative to liposomes for Dox delivery. Cyclic peptide cNGQGEQc-decorated polymersomes (cNGQ-PS) are easily prepared with a small size and high Dox loading. Dox-loaded cNGQ-PS (cNGQ-PS-Dox) shows superb stability with minimal drug leakage under physiological conditions while spontaneous disassembly and quick drug release in response to 10 mM glutathione. MTT assays, flow cytometry and confocal microscopy clearly display efficient receptor-mediated internalization of cNGQ-PS-Dox, fast intracellular drug release, and high antitumor activity in $\alpha_3\beta_1$ integrin-overexpressing A549 lung cancer cells. Intriguingly, cNGQ-PS-Dox presents a remarkably high maximum-tolerated dose of over 100 mg/kg, over 6-fold higher than Lipo-Dox. The *in vivo* pharmacokinetics and biodistribution studies reveal that cNGQ-PS-Dox has a long circulation time and significantly enhanced tumor accumulation (8.60%ID/g) as compared to Lipo-Dox and non-targeting PS-Dox controls. Notably, cNGQ-PS-Dox shows superior treatment of both subcutaneous and orthotopic A549 human lung cancer bearing nude mice to Lipo-Dox, resulting in effective tumor suppression, significantly improved survival time, and markedly reduced adverse effects. cNGQ-PS appears to be a clinically viable system for targeted lung cancer chemotherapy.



## 1. Introduction

Cancer nanomedicines have promised to offer a better treatment for different human malignancies [1–4]. Pegylated liposomal doxorubicin (Lipo-Dox) is the first clinically approved nanomedicine used to treat a variety of cancers including Kaposi's sarcoma, ovarian cancer, multiple myeloma, and metastatic breast cancer [5–6]. The clinical success of Lipo-Dox benefits from its high Dox loading by the pH gradient method and effective stealth by PEGylation, which leads to long circulation time, improved biodistribution and therapeutic index, and reduced cardiotoxicity as compared to free Dox. Lipo-Dox shows, nevertheless, low tumor selectivity and distinct adverse effects like hand-foot syndrome and stomatitis [7]. It is interesting to note that despite their immense promise and remarkable advance, very few cancer nanomedicines have translated to the clinics [8–9]. Moreover, current clinical cancer nanomedicines including Lipo-Dox display only modest survival benefits [10–12].

Polymersomes are tough vesicles self-assembled from amphiphilic diblock copolymers [13–15]. Like liposomes, polymersomes are able to encapsulate both hydrophobic and hydrophilic pharmaceuticals [16–18]. Interestingly, polymersomes are intrinsically stealthy, significantly more robust and versatile as compared to liposomes, and amenable to facile engineering of the vesicular membrane and surface [19–22]. For example, stimuli-sensitive polymersomes that respond to different signals like pH [23–24], redox potential [25–26], temperature [27–28], enzyme [29] or magnetic field [30] have been developed to achieve enhanced temporal and spatial control over drug release. Targeting polymersomes whose surfaces are functionalized with various biomolecules such as peptide [31–32], antibody [33], folate [34], hyaluronic acid [35], and acupa [36] have been explored to accomplish targeted drug delivery. To further enhance their stability in circulation, the membrane of polymersomes has been chemically crosslinked [25,37–38]. It should be noted, however, that reported multifunctional polymersomes typically involve sophisticated design and fabrication [3,39–40]. The lessons from the few clinically successful nanomedicines show that besides efficacy and safety, simplicity and cost play a decisive role in their translation into therapeutic products [41–43].

In this study, we have designed and developed $\alpha_3\beta_1$ integrin specific, redox-responsive and reversibly crosslinked biodegradable polymersomes, which are multifunctional and yet simple and easy to prepare, for efficient loading and targeted delivery of Dox to subcutaneous as well as orthotopic A549 human lung cancer xenografts in nude

* Corresponding authors.
*E-mail addresses:* fhmeng@suda.edu.cn (F. Meng), zyzhong@suda.edu.cn (Z. Zhong).

http://dx.doi.org/10.1016/j.jconrel.2016.08.022
0168-3659/

mice (Scheme 1). These multifunctional polymersomes are *co*-self-assembled from poly(ethylene glycol)-*b*-poly (trimethylene carbonate-co-dithiolane trimethylene carbonate) (PEG-P(TMC-DTC)) and cNGQGEQc-functionalized PEG-P(TMC-DTC) (cNGQ-PEG-P(TMC-DTC)). The proprietary functional monomer, dithiolane trimethylene carbonate (DTC), can be easily synthesized [44]. Notably, the membrane-forming hydrophobic block consists of poly(trimethylene carbonate) backbone, which is known biodegradable and biocompatible [45], and pendant dithiolane ring, which is analogous to lipoic acid, a natural antioxidant produced in human being and a drug used for treatment of diabetes and Alzheimer's disease [46]. We have shown previously that reversibly crosslinked nanoparticles based on dextran-lipoic acid have superior stability with inhibited drug release under physiological conditions while are rapidly de-crosslinked and de-stabilized in the cytoplasm of cancer cells [47]. cNGQ peptide has shown a high and specific affinity to $\alpha_3\beta_1$ integrins that are overexpressed in A549 human lung cancer cells [48]. Our results show that Dox-loaded cNGQ-decorated polymersomes afford superior treatment of orthotropic human lung cancers to Lipo-Dox.

## 2. Materials and methods

### 2.1. Materials

Methoxy poly(ethylene glycol) (MeO-PEG-OH, $M_n$ = 5.0 kg/mol, PDI = 1.03, Fluka) and N-hydroxysuccinimide activated poly(ethylene glycol) (NHS-PEG-OH, $M_n$ = 6.5 kg/mol, PDI = 1.04, Suzhou Nord Derivatives Pharm-tech Co. Ltd) were dried by azeotropic distillation from anhydrous toluene. Toluene and dichloromethane (DCM) were dried by refluxing over $CaH_2$ and distilled prior to use. Trimethylene carbonate (TMC) was recrystallized over dry toluene. Zinc bis [bis(trimethylsilyl) amide] (97%, Aldrich), cyclic peptide C(NGQGEQ) (cNGQ, 98%, China Peptides Co., Ltd.), glutathione (GSH, 99%, Roche), Cy7-NHS (Beijing Fanbo biochemicals) and doxorubicin hydrochloride (DOX·HCl, >99%, Beijing Zhongshuo Pharmaceutical Technology Development) were used as received. Dithiolane trimethylene carbonate (DTC) was synthesized as our previous report [44].

### 2.2. Characterization

The chemical structures of the polymers were characterized using $^1$H NMR on a Unity Inova 400 spectrometer operating at 400 MHz or Agilent DD2 operating at 600 MHz. The chemical shifts were calibrated against residual solvent signal. The molecular weight and polydispersity of copolymers were determined by a Waters 1515 gel permeation chromatograph (GPC) instrument equipped with two linear PLgel columns (500 Å and Mixed-C) following a guard column and a differential refractive-index detector. The measurements were performed using DMF as an eluent at a flow rate of 1.0 mL/min at 30 °C and a series of narrow polystyrene standards for the calibration of the columns. The size and size distribution of polymersomes were determined at 25 °C using dynamic light scattering (DLS, Zetasizer Nano-ZS, Malvern Instruments) equipped with a 633 nm He-Ne laser using back-scattering detection. Zeta potential measurements were carried out using Zetasizer Nano-ZS instrument (Malvern) equipped with a standard capillary electrophoresis cell. The measurements were performed in triplicate.

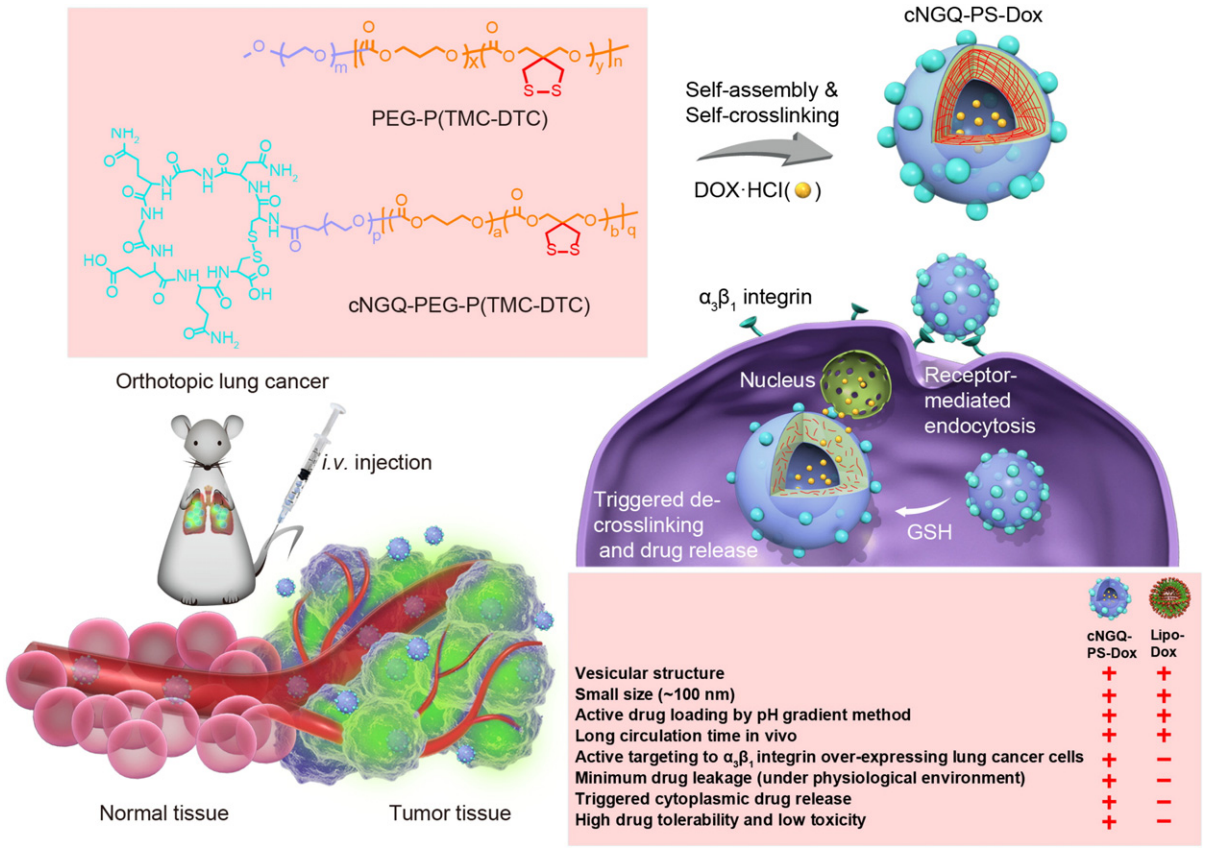


**Scheme 1.** cNGQ-PS-Dox as a better alternative to clinically used Lipo-Dox. cNGQ-PS-Dox while sharing basic characteristics of Lipo-Dox including a vascular structure, small size, high drug loading and long circulation time presents several unique features such as easy synthesis, inhibited premature drug release, high tumor selectivity and accumulation, efficient intracellular drug release, low systemic toxicity and high therapeutic index.

Transmission electron microscopy (TEM) was performed using a Tecnai G220 TEM operated at an accelerating voltage of 120 kV. The samples were prepared by dropping 10 μL of 0.2 mg/mL polymersome suspension on the copper grid followed by staining with phosphotungstic acid (1 wt.%). The CLSM images were taken on a confocal laser scanning microscope (TCS SP5). The crosslinking polymersome dectection was performed using UV (UH5300 Hitachi) spectrum and calibrated with PEG-PTMC polymersomal nanoparticle dispersions.

### 2.3. Synthesis of PEG-P(TMC-DTC) and cNGQ-PEG-P(TMC-DTC) diblock copolymers

PEG-P(TMC-DTC) was synthesized by ring-opening copolymerization of TMC and DTC using MeO-PEG-OH as a macro-initiator and zinc bis[bis(trimethylsilyl)amide] as a catalyst. Briefly, in a glove-box under a nitrogen atmosphere, zinc bis[bis(trimethylsilyl)amide] (29 mg, 75 μmol) was quickly added to a stirred solution of MeO-PEG-OH ($M_n$ = 5.0 kg/mol, 0.50 g, 100 μmol), TMC (2.0 g, 19.2 mmol) and DTC (0.50 g, 2.60 mmol) in DCM (10.0 mL). The reaction vessel was sealed and placed into an oil-bath thermostated at 40 °C. The polymerization was allowed to proceed with magnetic stirring for 48 h. PEG-P(TMC-DTC) copolymer was isolated by twice precipitation from cold diethyl ether, filtration and drying *in vacuo* at room temperature (r.t.). Yield: 86.3%. $^1$H NMR (400 MHz, $CDCl_3$): PEG: δ 3.38, 3.65; TMC: δ 4.24, 2.05; DTC: δ 4.32, 3.02. $M_n$ ($^1$H NMR) = 29.8 kg/mol, $M_n$ (GPC) = 35.5 kg/mol, PDI = 1.42.

cNGQ-PEG-P(TMC-DTC) diblock copolymer was synthesized in two steps. Firstly, NHS-PEG-P(TMC-DTC) was obtained as described above except that NHS-PEG-OH ($M_n$ = 6.5 kg/mol) was used as a macro-initiator. Yield: 85.7%. $^1$H NMR (400 MHz, $CDCl_3$): PEG: δ 3.64; TMC moieties: δ 4.24, 2.06; DTC moieties: δ 4.32, 3.02, NHS moieties: δ 2.52. $M_n$ ($^1$H NMR) = 30.0 kg/mol, $M_n$ (GPC) = 38.9 kg/mol, PDI = 1.38. Secondly, NHS-PEG-P(TMC-DTC) reacted with cNGQ peptide. Briefly, NHS-PEG-P(TMC-DTC) (0.3 g, 0.010 mmol) and cNGQ (13 mg, 0.015 mmol) dissolved 4 mL of DMF and the reaction proceeded for 24 h at rt. The final product, cNGQ-PEG-P(TMC-DTC), was isolated through dialysis (MWCO 7000) against deionized water for 48 h followed by lyophilization. Yield: 88.6%. $^1$H NMR (600 MHz, DMSO-$d_6$): PEG: δ 3.51; TMC: δ 4.23, 1.94; DTC: δ 4.13, 2.99; cNGQ: δ 5.08–7.72. The degree of cNGQ conjugation was determined to be 85% by Micro BCA protein assay kit (Thermo scientific).

### 2.4. Preparation of cNGQ-PS

cNGQ-PS were prepared from PEG-P(TMC-DTC) and cNGQ-PEG-P(TMC-DTC) *via* solvent exchange method. Typically, under stirring 900 μL of PB (10 mM, pH 7.4) was added dropwise to 100 μL of DMF solution of PEG-P(TMC-DTC) and cNGQ-PEG-P(TMC-DTC) (10.0 mg/mL) followed by extensive dialysis against (Spectra/Pore, MWCO 7000) PB for 12 h. cNGQx-PS-Dox, wherein x represents the weight percentage of cNGQ-PEG-P(TMC-DTC), was finally obtained by further incubating in a shaking-bed for 24 h at 37 °C. The colloidal stability of cNGQ-PS-Dox at low concentration or in the presence of 10 mM GSH was investigated by tracking the size change using DLS.

### 2.5. Loading and reduction-triggered release of DOX·HCl

DOX·HCl was loaded into cNGQ-PS by a pH-gradient method. Briefly, 4 mL of citric acid buffer (10 mM, pH 4.0) was dropwise added to 1 mL of DMF solution of PEG-P(TMC-DTC)/cNGQ-PEG-P(TMC-DTC) (10.0 mg/mL) within 10 min. After stirring 30 min, the pH value was quickly adjusted to 8.0 using disodium hydrogen phosphate solution (4 M). The solution was divided into three aliquots and 20, 30 or 40 μL of DOX·HCl solution in water (5 mg/mL) was added, corresponding to a theoretical drug loading content (DLC) of 9.1, 13.0 and 16.7 wt.%, respectively. After stirring at 37 °C for 5 h, the polymersomes were extensively dialyzed against PB (10 mM, pH 7.4) with at least 5 times change of dialysis medium. cNGQ-PS-Dox was finally obtained by further incubating in a shaking-bed overnight at 37 °C. The whole procedure was performed in the dark. For determination of drug loading content (DLC) and drug loading efficiency (DLE), the samples were lyophilized, dissolved in DMF and analyzed with fluorometry (ex. 480 nm, em. 560 nm). DLC and DLE were calculated according to the following formula based on a calibration curve obtained with DOX·HCl/DMF of known DOX·HCl concentrations:

$$\text{DLC (wt.\%)} = (\text{weight of loaded drug/total weight of loaded drug and polymer}) \times 100$$

$$\text{DLE (\%)} = (\text{weight of loaded drug/weight of drug in feed}) \times 100$$

The *in vitro* drug release from cNGQ-PS-Dox, PS-Dox and Lipo-Dox polymersomes was studied at a low polymersome concentration of 30 mg/L using dialysis tube (Spectra/Pore, MWCO 12000) at 37 °C in two different media, *i.e.* PB (10 mM, pH 7.4) and PB (10 mM, pH 7.4) containing 10 mM GSH. In order to acquire sink conditions, drug release studies were performed using 600 μL of cNGQ-PS-Dox and PS-Dox to dialyze against 25 mL of the corresponding medium. At desired time intervals, 5.0 mL of release medium was taken out and replenished with an equal volume of fresh medium. The DOX·HCl released was quantified using fluorometry. The release experiment was conducted in triplicate, and the results presented were the average data with standard deviations.

### 2.6. MTT assays

The cytotoxicity of cNGQ-PS and cNGQ-PS-Dox was evaluated using MTT assays in $\alpha_3\beta_1$ integrin receptor overexpressing A549 human lung cancer cells. The cells were plated in a 96-well plate ($5 \times 10^3$ cells/well) using 1640-RPMI medium for 24 h. cNGQ-PS-Dox, PS-Dox or Lipo-Dox in 10 μL of PBS was added, the cells were incubated for 4 h, and the medium was aspirated and replaced by fresh medium. The cells were incubated for 44 h, 3-(4,5-dimethylthiazol-2-yl)-2,5-diphenyl tetrazoliumbromide (MTT) solution in PBS (10 μL, 5 mg/mL) was added, and the cells were cultured for another 4 h. The supernatant was carefully aspirated, the MTT-formazan generated by live cells was dissolved in 150 μL of DMSO, and the absorbance at 492 nm of each well was measured using a microplate reader. The absorbance of the control wells containing DMSO only was used as a background signal. The relative cell viability was determined by comparing the absorbance at 492 nm with cells cultured in 1640-RPMI medium (without exposure to polymersome). The competitive inhibition experiments were performed by pretreating A549 cells with free cNGQ (200 μg/mL) for 2 h before adding cNGQ-PS-Dox. The cytotoxicity of blank cNGQ-PS was assessed in a similar way except that cells were incubated with cNGQ-PS for 48 h. The data are presented as average ± SD (n = 4).

### 2.7. Confocal microscope

A549 cells cultured on microscope slides in 24-well plates ($1 \times 10^5$ cells/well) were incubated with cNGQ-PS-Dox, PS-Dox or DOX-LPs in 50 μL of PBS (DOX·HCl dosage: 10 μg/mL) at 37 °C. After 4 h incubation, the medium was aspirated and replaced by fresh medium, and the cells were further incubated for another 4 h. The culture medium was removed, the cells were fixed with 4% paraformaldehyde solution for 15 min, the cytoskeleton was stained with fluorescein isothiocyanate labeled phalloidin (phalloidin-FITC), and the cell nuclei were stained with 4′,6-diamidino-2-phenylindole (DAPI) for 10 min. The fluorescence images were obtained using a confocal microscope (TCS SP5).

### 2.8. Flow cytometry assays

A549 cells seeded in a 6-well plate ($1 \times 10^6$ cells/well) were incubated with cNGQx-PS-Dox (x: 10%, 20% and 30%) or Lipo-Dox in 500 μL of PBS (DOX·HCl concentration: 10 μg/mL) at 37 °C for 4 h. The cells were digested by 0.25% (w/v) trypsin and 0.03% (w/v) EDTA. The suspensions were centrifuged at 1000 ×*g* for 3 min, washed twice with PBS, and then re-suspended in 500 μL of PBS. Fluorescence histograms were immediately recorded with a BD FACS Calibur flow cytometer (Becton Dickinson, USA) and analyzed using Cell Quest software based on 10,000 gated events. The gate was arbitrarily set for the detection of FITC fluorescence.

### 2.9. Animal models

All animal procedures were handled under protocols approved by Soochow University Laboratory Animal Center and the Animal Care and Use Committee of Soochow University. Female nude mice (18–22 g) were inoculated subcutaneously on the right flank with A549 human lung cancer cells ($5 \times 10^6$ per mouse). Mice with tumor sizes of *ca.* 150–200 $mm^3$ were used for imaging and biodistribution studies and with tumor sizes of *ca.* 30–50 $mm^3$ for therapeutic studies. Orthotopic A549 lung tumor model was acquired by injecting 100 μL of bioluminescent A549-Luc cell suspension ($5 \times 10^6$ cells). The growth of tumor was monitored by imaging system in live animals.

### 2.10. In vivo pharmacokinetics and biodistribution

For pharmacokinetic studies, cNGQ-PS-Dox, PS-Dox or Lipo-Dox (7.5 mg DOX·HCl equiv./kg) in 150 μL of PB was intravenously injected into nude mice *via* the tail vein (n = 3). At prescribed time points post injection, *ca.* ~10 μL of blood was withdrawn from the tail vein of nude mice. The blood samples upon withdrawing were immediately dissolved in 0.1 mL of lysis buffer (1% Triton X-100) with brief signification. DOX·HCl was extracted by incubating blood samples in 0.5 mL of extraction solution (DMF containing 50 mM HCl and 20 mM DTT) at −20 °C overnight followed by centrifugation (14.8 krpm, 30 min). The DOX·HCl level in the supernatant was determined by fluorometry.

For *in vivo* biodistribution studies, tumor-bearing mice were randomly grouped and intravenously injected with Cy7-labeled cNGQ-PS or Cy7-labeled PS in 150 μL PB *via* tail vein. At predetermined time points (0, 1, 4, 12, 24 and 48 h) post *i.v.* injection, the mice were anesthetized with isoflurane and the fluorescent images were obtained using a near-infrared fluorescence imaging system (IVIS Lumina II) at Ex 747 nm and Em 774 nm. For *ex vivo* imaging, a single dose of cNGQ-PS-Dox, PS-Dox or Lipo-Dox in 150 μL PBS was administrated intravenously *via* the tail vein (7.5 mg DOX·HCl equiv./kg) into mice bearing A549 subcutaneous tumor xenograft. At 8 h post injection, the tumor-bearing mice were sacrificed. Fluorescence images were acquired with the fluorescence imaging system. To further quantify DOX·HCl levels, major organs and tumor block were homogenized in 0.6 mL of 1% Triton X-100 with a homogenizer (IKA T25) at 18,000 rpm for 10 min. DOX·HCl was extracted by DMF solution containing 50 mM HCl and 20 mM DTT. The amount of DOX·HCl was determined by fluorescence measurement.

### 2.11. In vivo antitumor efficacy

The mice were weighed and randomly divided into four groups (n = 6, one mouse for histological analysis and the other five for monitoring the body weights and survival rates). cNGQ-PS-Dox, PS-Dox, Lipo-Dox or PBS were intravenously injected *via* tail vein every 4 days (dosage: 7.5 mg DOX·HCl equiv./kg). The relative tumor volume was calculated as $V/V_0$ ($V_0$ is the tumor volume at day 0). The relative body weights of mice were weighed and normalized to their initial weights. When the treatment was terminated, one mouse of each group was sacrificed by cervical vertebra dislocation. The major organs and tumor were isolated, fixed with 4% paraformaldehyde solution and embedded in paraffin. The sliced organ tissues mounted on the glass slides were stained by hematoxylin and eosin (H&E) and TUNEL and observed by a digital microscope (Olympus BX41).

### 2.12. Blood biochemistry analyses

The healthy Balb/c mice were weighed and randomly divided into three groups (n = 5). cNGQ-PS-Dox, PS-Dox or PBS were intravenously injected *via* tail vein (dosage: 10 mg DOX·HCl equiv./kg). About 1 mL of blood was withdrawn from the tail vein of mice at 24 h post injection, and immediately centrifuged at 5000 rpm for 3 mins to collect blood serum for blood biochemistry analysis. The blood levels of alkaline phosphatase (ALP), aspartate aminotransferase (AST), alanine aminotransferase (ALT) and serum albumin (ALB) were determined.

### 2.13. Statistical analysis

Data were expressed as mean ± s.d. Differences between groups were assessed using the paired, two-sided Student's *t*-test. $^*p < 0.05$ was considered significant, and $^{**}p < 0.01$, $^{***}p < 0.001$ were considered highly significant.

## 3. Results and discussion

### 3.1. Synthesis of PEG-P(TMC-DTC) and cNGQ-PEG-P(TMC-DTC) diblock copolymers

PEG-P(TMC-DTC) block copolymer was readily prepared by ring-opening copolymerization of trimethylene carbonate (TMC) with dithiolane trimethylene carbonate (DTC) using MeO-PEG-OH ($M_n$ = 5.0 kg/mol) as a macro-initiator and zinc bis[bis(trimethylsilyl)amide] as a catalyst in $CH_2Cl_2$ at 40 °C (Scheme 2). $^1$H NMR spectrum showed besides signals attributable to PEG (δ 3.65, 3.38) also peaks due to TMC moieties (δ 4.24, 2.05) and DTC moieties (δ 4.32, 3.02) (Fig. 1). The molecular weight of P(TMC-DTC) block was determined to be 24.2 kg/mol, composed of 19.4 kg/mol TMC and 4.8 kg/mol DTC units, by comparing the integrals of signals at δ 2.05 (methylene protons of TMC moieties) and 3.02

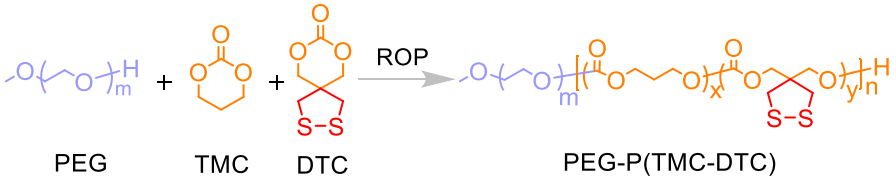


**Scheme 2.** Synthesis of PEG-P(TMC-DTC) by ring-opening polymerization. Conditions: $CH_2Cl_2$, 40 °C, 48 h.

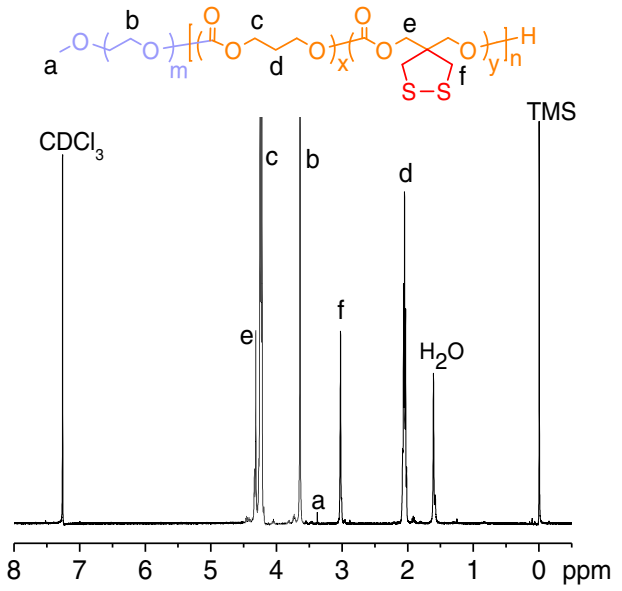


**Fig. 1.** $^1$H NMR spectrum ($CDCl_3$, 400 MHz) of PEG-P(TMC-DTC).

(dithiolane methylene protons of DTC moieties) to 3.65 (methylene protons of PEG main chain), respectively. GPC revealed that resulting copolymer had a polydispersity of 1.42 and an $M_n$ of 35.5 kg/mol, close to that determined by $^1$H NMR (29.2 kg/mol) as well as the design (29.8 kg/mol), confirming controlled synthesis of PEG-P(TMC-DTC) diblock copolymer.

cNGQ-PEG-P(TMC-DTC) diblock copolymer was synthesized using NHS-PEG-OH ($M_n$ = 6.5 kg/mol) as a macro-initiator followed by conjugating with cNGQ peptide (Scheme 3). $^1$H NMR analysis showed that cNGQ-PEG-P(TMC-DTC) had an $M_n$ of 6.5-(19.6–4.9) kg/mol (**Fig. S1**), similar to PEG-P(TMC-DTC). The signals assignable to the amide protons of cNGQ peptide were clearly detected at $\delta$ 5.08–7.72. The degree of cNGQ conjugation was determined to be 85% by Micro BCA protein assay kit (Thermo scientific). The PEG in cNGQ-PEG-P(TMC-DTC) was designed longer than that in PEG-P(TMC-DTC) to achieve optimal exposure of cNGQ targeting ligand.

### *3.2. Preparation of $\alpha_3\beta_1$ integrin specific multifunctional biodegradable polymersome*

Interestingly, PEG-P(TMC-DTC) and cNGQ-PEG-P(TMC-DTC) (w/w, 8/2) formed monodisperse polymersomes (cNGQ-PS) with a small size of *ca.* 105 nm and low PDI of 0.10, as shown by dynamic light scattering (DLS) (Fig. 2a). TEM micrograph confirmed that cNGQ-PS had a spherical vesicular structure. Remarkably, UV revealed complete disappearance of characteristic absorbance of dithiolane ring at 330 nm (**Fig. S2a**), indicating that cNGQ-PS are self-crosslinked during work-up. In accordance, cNGQ-PS showed excellent colloidal stability over extensive dilution, against 10% FBS, and in DMEM cell culture medium (**Fig. S2b**). Under an intracellular mimicking reductive condition containing 10 mM GSH, however, they quickly swelled to over 670 nm in 12 h (**Fig. S2c**), signifying that they possess a fast bioresponsivity [40].

DOX·HCl was conveniently loaded into cNGQ-PS by the pH-gradient method, which is used for Lip-Dox [49]. Notably, cNGQ-PS-Dox exhibited a high drug loading content (DLC) of 11.4 wt.% and maintained a small size of 118 nm (Table 1). Zeta potential measurements showed that cNGQ-PS-Dox and PS-Dox had a neutral surface charge of +0.9 and +0.3 mV, respectively. The *in vitro* drug release studies showed that under physiological condition <16.0% drug was released in 24 h from cNGQ-PS-Dox, which was far lower than 66.4% observed for Lipo-Dox (Fig. 2b), indicating that cNGQ-PS-Dox is significantly more stable and has less drug leakage than Lipo-Dox. Strikingly, cNGQ-PS-

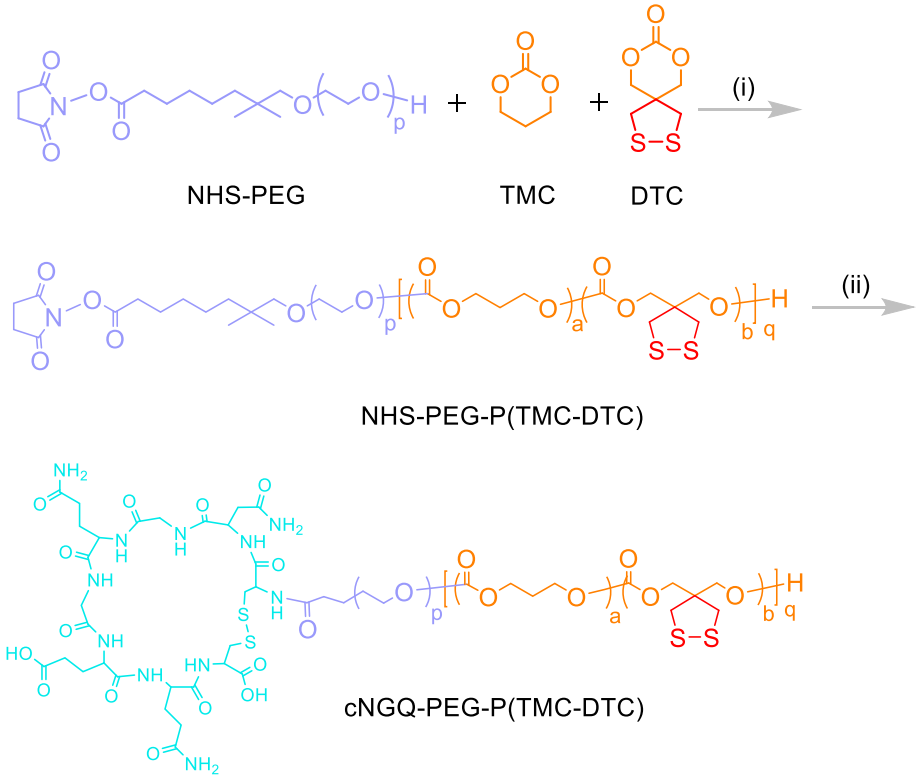


**Scheme 3.** Synthesis of cNGQ-PEG-P(TMC-DTC). Conditions: (i), $CH_2Cl_2$, 40 °C, 48 h; (ii) cNGQGEQc, r.t., 48 h.

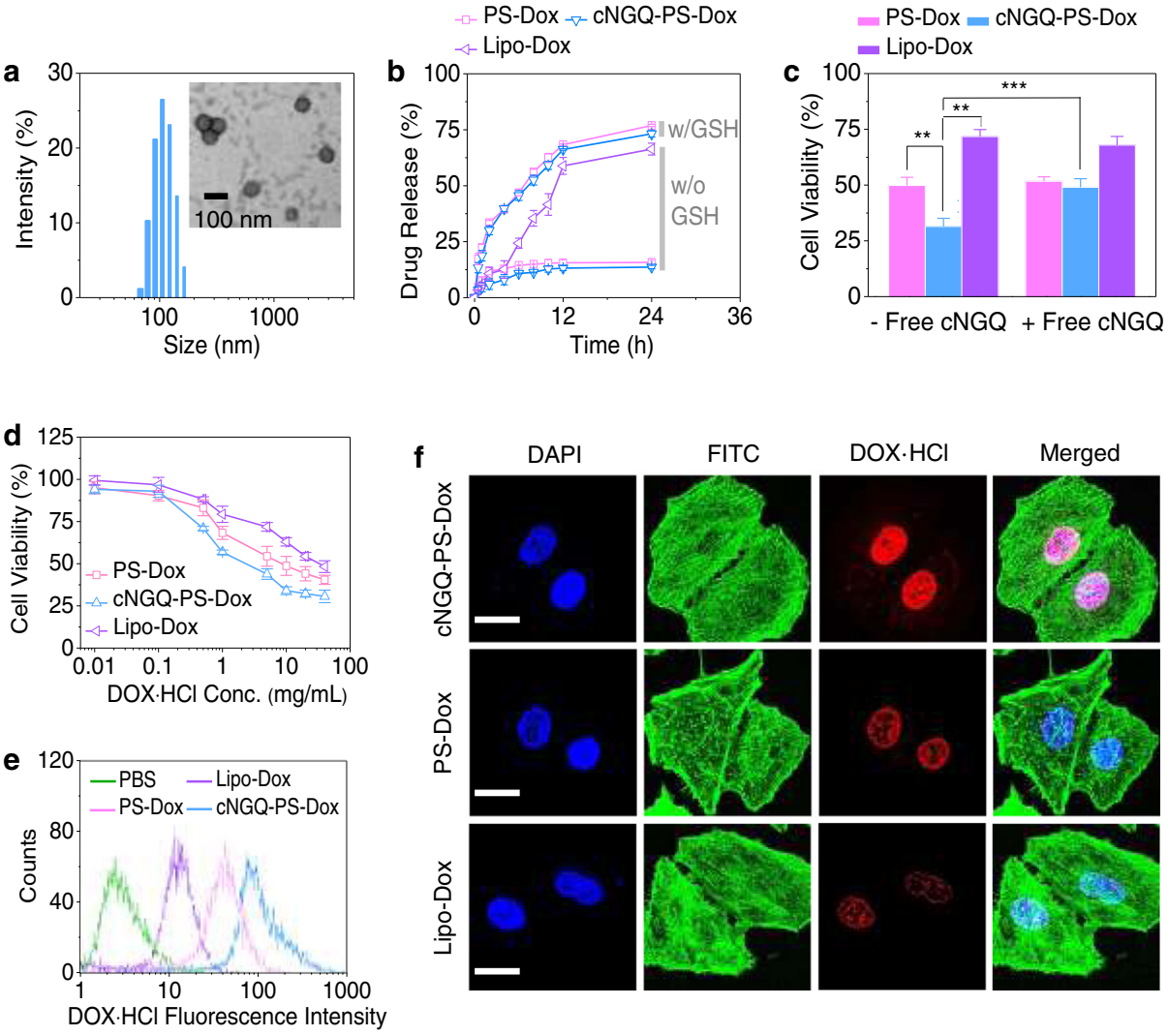


**Fig. 2.** Characterizations of cNGQ-PS and cNGQ-PS-Dox. (a) Size distribution of cNGQ-PS measured by DLS (inset: TEM image); (b) *In vitro* drug release profiles of cNGQ-PS-Dox, PS-Dox and Lipo-Dox in PB at 37 °C with or without 10 mM GSH; (c) Competitive experiments performed by pre-treating A549 cells with free cNGQ (200 μg/mL) for 2 h before adding cNGQ-PS-Dox. The cells were incubated for 4 h with cNGQ-PS-Dox, medium was removed and replenished with fresh medium, and cells were further cultured for another 44 h. PS-Dox and Lipo-Dox were used as controls; (d) The antitumor activity of cNGQ-PS-Dox, PS-Dox and Lipo-Dox towards A549 cells determined by MTT assays. The data are presented as mean ± SD (n = 4); (e) Flow cytometry studies of A549 cells following 4 h incubation with cNGQ-PS-Dox, PS-Dox or Lipo-Dox; (f) CLSM images of A549 cells after 4 h incubation with cNGQ-PS-Dox, PS-Dox or Lipo-Dox followed by another 4 h culture in fresh medium. For each panel, the images from left to right were cell nuclei stained by DAPI (blue), cytoskeleton stained by phalloidin-FITC (green), DOX·HCl (red), and overlays of the three images, and the bar represents 25 μm. For c, e and f, the drug dosage was 10.0 μg DOX·HCl equiv./mL.

Dox exhibited markedly accelerated drug release (73.2% in 24 h) in the presence of 10 mM GSH under otherwise the same conditions, supporting its superior control of drug release to Lipo-Dox.

**Table 1**
Characterization of PS-Dox and cNGQ-PS-Dox in PB buffer.

| Polymersomes | DLC (wt.%) | | DLE[a] (%) | Size[b] (nm) | PDI[b] |
|---|---|---|---|---|---|
| | Theory | Determined[a] | | | |
| PS-Dox | 9.1 | 7.4 | 80.3 | 95 ± 4 | 0.11 |
| | 13.0 | 10.0 | 74.5 | 103 ± 3 | 0.12 |
| | 16.7 | 12.2 | 68.4 | 115 ± 5 | 0.15 |
| cNGQ-PS-Dox | 9.1 | 7.3 | 79.1 | 98 ± 3 | 0.10 |
| | 13.0 | 10.3 | 76.8 | 105 ± 3 | 0.13 |
| | 16.7 | 11.4 | 64.3 | 118 ± 4 | 0.15 |

[a] Determined by fluorometry (ex. 488 nm and em. 590 nm).
[b] Determined by DLS (10 mW He-Ne laser, 633 nm wavelength) at 25 °C in PB buffer (pH 7.4, 10 mM) at a concentration of 1.0 mg/mL.

### 3.3. Selective internalization by A549 lung cancer cells

To investigate the cytotoxicity of blank cNGQ-PS and cNGQ-PS-Dox, MTT assays were carried out in $\alpha_3\beta_1$ integrin overexpressing A549 cells. The results revealed that blank cNGQ-PS was non-cytotoxic even at a high concentration of 1.0 mg/mL (**Fig. S3a**), corroborating its excellent biocompatibility. Notably, cNGQ-PS-Dox showed strong and cNGQ-dependent toxicity to A549 cells (**Fig. S3b**), in accordance with its active targeting effect. Fig. 2c shows clearly that both cNGQ-PS-Dox and PS-Dox were much more potent than Lipo-Dox. The competitive inhibition experiments further confirmed that cNGQ-PS-Dox is taken up by A549 cells *via* a receptor-mediated mechanism. The half-maximal inhibitory concentration ($IC_{50}$) of cNGQ-PS-Dox, PS-Dox and Lipo-Dox was determined to be 2.56, 8.78, and 15.21 μg Dox·HCl equiv./mL, respectively (Fig. 2d). The superior antitumor activity of cNGQ-PS-Dox to Lipo-Dox is likely because of its selective and efficacious internalization by A549 cells and fast intracellular drug release. To confirm this, we have

performed flow cytometry and confocal laser scanning microscopy (CLSM) analyses. Fig. 2e shows that PS-Dox and in particular cNGQ-PS-Dox afforded greatly enhanced Dox level in A549 cells as compared to Lipo-Dox. Flow cytometry with Cy5-labled polymersomes demonstrated obviously more efficient cellular uptake of Cy5-cNGQ-PS than Cy5-PS by A549 cells (**Fig. S5**). Moreover, strong DOX fluorescence was observed in the nuclei of A549 cells following 4 h incubation with cNGQ-PS-Dox and further 4 h culture in fresh media, which was significantly stronger than those treated with PS-Dox and Lipo-Dox (Fig. 2f), verifying efficient cellular uptake and nuclei release of DOX·HCl into A549 cells.

### 3.4. In vivo pharmacokinetics and biodistribution

The *in vivo* pharmacokinetic studies showed that cNGQ-PS-Dox had a long circulation time with an elimination half life ($t_{1/2,\beta}$) of 4.99 h (Fig. 3a), which is though shorter than Lipo-Dox ($t_{1/2,\beta}$ = 8.96 h) significantly longer than common micellar and polymersomal systems [50]. In order to monitor their biodistribution *in vivo*, we labeled PS and cNGQ-PS with Cy7. Fig. 3b shows that Cy7-labeled cNGQ-PS accumulated at subcutaneous A549 human lung tumor in mice 1 h post injection. The tumor accumulation peaked at 8 h and remained strong even at 48 h post injection. In comparison, Cy7-labeled PS (non-targeting control) revealed significantly less tumor accumulation, though cNGQ-PS and PS had similar circulation time. These results indicate that cNGQ peptide plays a critical role in achieving high tumor accumulation and retention. The *ex vivo* fluorescence images of the major organs and tumor blocks excised at 8 h post intravenous injection show that mice treated with cNGQ-PS-Dox had significantly stronger DOX fluorescence in the tumor than in the major organs including heart, liver, spleen, kidney and lung (Fig. 3c). In comparison, much weaker DOX fluorescence was observed in the tumor of mice treated with PS-Dox and Lipo-Dox. Moreover, Lipo-Dox exhibited strong drug accumulation in the lung and kidney. The quantitative measurements demonstrated that cNGQ-PS-Dox gave a remarkably high DOX·HCl tumor accumulation of 8.60% ID/g, which was about 2.4- and 3.1-fold higher than that for PS-Dox and Lipo-Dox, respectively (Fig. 3d). Notably, reportedly <5% ID/g drug accumulation is detected in the tumor for nanotherapeutics [51]. The exceptional tumor drug level observed for cNGQ-PS-Dox likely results from its favorable stability, small size, long circulation time and active tumor targeting effect. The graph of tumor-to-normal tissue (T/N) ratios shows that cNGQ-PS-Dox had 2.7–6.8 and 4.9–16.6 folds better tumor selectivity than PS-Dox and Lipo-Dox, respectively (**Fig. S6**). It is evident, therefore, that cNGQ-PS-Dox is superior in tumor selectivity, accumulation and retention to Lipo-Dox.

### 3.5. Targeted treatment of subcutaneous A549 human lung tumor

The therapeutic studies in nude mice bearing subcutaneous A549 human lung tumor xenografts revealed that cNGQ-PS-Dox completely inhibited tumor growth at a dosage of 7.5 mg DOX·HCl equiv./kg (Fig. 4a). PS-Dox could partially suppress tumor growth. Lipo-Dox though effectively inhibited tumor growth caused significant body weight loss compared with PBS groups (Fig. 4b), indicating a high systemic toxicity. In contrast, no body weight loss was observed for mice treated with cNGQ-PS-Dox and PS-Dox, confirming that they have little adverse effects. Remarkably, Kaplan–Meier survival curves showed that the mice treated with cNGQ-PS-Dox all survived within an experiment period of 68 days (Fig. 4c). The mice treated with PS-Dox showed also a longer median survival time than those with Lipo-Dox (40 *versus* 24 days). The therapeutic outcome of Lipo-Dox is largely compromised by its pronounced side effects. The histological analyses using H&E and TUNEL staining revealed that cNGQ-PS-Dox caused widespread necrosis in the tumor tissue while little damage to the liver, kidney and heart (Fig. 4d). In contrast,

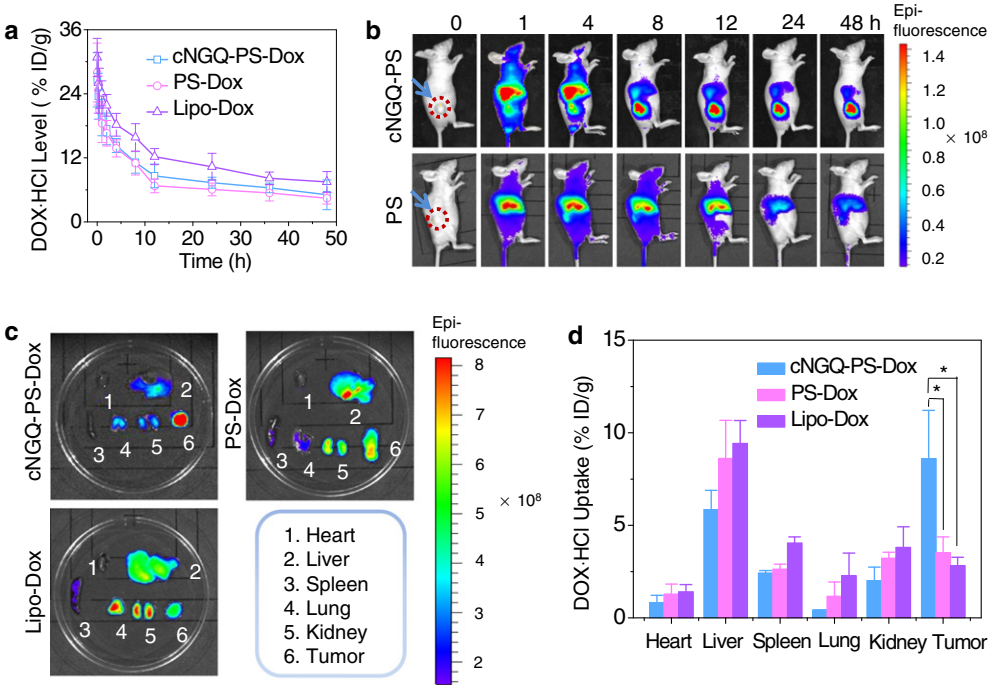


**Fig. 3.** *In vivo* pharmacokinetics and biodistribution. (a) *In vivo* pharmacokinetics in mice. DOX·HCl levels were determined by fluorescence spectroscopy, and expressed as injected dose per gram of tissue (%ID/g). Data are presented as mean ± SD (n = 3); (b) *In vivo* fluorescence images of A549 subcutaneous tumor-bearing nude mice at different time points following *i.v.* injection of Cy7-labeled cNGQ-PS or Cy7-labeled PS; (c) *Ex vivo* fluorescence images of DOX·HCl in major organs and tumor blocks excised at 8 h post intravenous injection; (d) Quantification of DOX·HCl accumulated in different organs and tumor using fluorescence spectroscopy. Data are presented as mean ± SD (n = 3, student's test, $^*p < 0.05$).

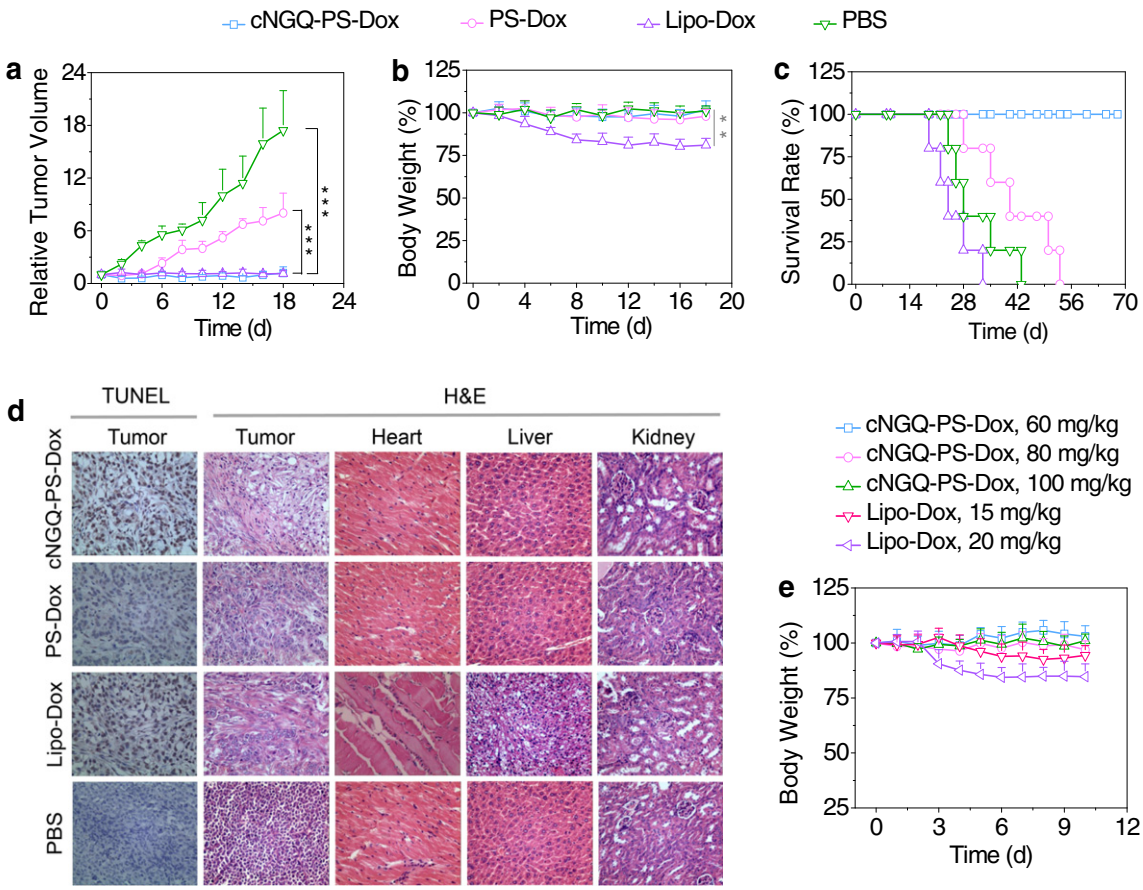


**Fig. 4.** *In vivo* antitumor performance in subcutaneous A549 human lung tumor-bearing nude mice (n = 5, student's test, $^{***}p < 0.001$). (a) Relative tumor volume of mice treated with cNGQ-PS-Dox, PS-Dox, Lipo-Dox and PBS, respectively. The drug was iv administrated on day 0, 4, 8, and 12 (dosage: 7.5 mg DOX·HCl equiv./kg, in 0.15 mL PBS); (b) Body weight change of mice in different groups within 18 d (n = 5, student's test, $^{**}p < 0.01$); (c) Survival rates of mice in different groups within 68 d; (d) The histological analyses of TUNEL stained sections of tumor and H&E stained sections of tumor, heart, liver and kidney, which were excised from tumor-bearing mice following 18 days of treatment. The images were obtained under Olympus BX41 microscope using a 40× objective; (e) MTD studies of cNGQ-PS-Dox and Lipo-Dox in tumor-free nude mice (n = 5).

Lipo-Dox instigated significant hepatotoxicity and nephrotoxicity. Intriguingly, cNGQ-PS-Dox exhibited a remarkably high maximum-tolerated dose (MTD) of over 100 mg DOX equiv./kg, which was at least 6 times higher than Lipo-Dox (Fig. 4e). The soaring tolerability of cNGQ-PS-Dox can be attributed to its inhibited drug leakage, favorable biodistribution, and reduced non-specific cellular uptake [52]. The high MTD of cNGQ-PS-Dox affords an extremely broad therapeutic window, which is a remarkable advantage for its clinical applications [53].

### 3.6. Targeted treatment of orthotopic A549 human lung tumor

We further investigated the targetability and therapeutic efficacy of cNGQ-PS-Dox using the orthotopic human lung tumor model. To facilitate monitoring of tumor progression, bioluminescent A549-luciferase (A549-Luc) cells expressing a luciferase reporter were used. Remarkably, cNGQ-PS-Dox showed effective suppression of tumor growth (Fig. 5a). The non-targeting PS-Dox also retarded tumor progression though less effective than cNGQ-PS-Dox. The quantification of bioluminescence in the lungs displayed significantly lower luminescence level in the mice treated with cNGQ-PS-Dox than those with PS-Dox and PBS controls (Fig. 5b). The *ex vivo* luminescence images of the lungs excised on day 16 further confirmed diminishing tumor luminescence by cNGQ-PS-Dox. Lipo-Dox could also effectively suppress tumor growth, though led to significant body weight loss (Fig. 5c). In comparison, little body weight loss was observed for mice treated with both cNGQ-PS-Dox and PS-Dox. Notably, Kaplan–Meier survival curves showed that mice treated with cNGQ-PS-Dox all survived within an experiment period of 45 days while median survival times of 28, 20 and 23 days were observed for mice treated with PS-Dox, PBS and Lipo-Dox, respectively (Fig. 5d). The histological analyses using H&E staining revealed that the lung tissue of mice treated with cNGQ-PS-Dox was similar to that of tumor-free healthy mice (Fig. 5e). In contrast, mice treated with Lipo-Dox, PS-Dox and PBS displayed abundant neoplasm in the lung tissue. It should further be noted that in contrast to Lipo-Dox, cNGQ-PS-Dox caused little damage of heart, liver and kidney. The blood chemistry analyses showed that mice treated with Lipo-Dox and cNGQ-PS-Dox had similar blood levels of alkaline phosphatase (ALP), aspartate aminotransferase (AST), alanine aminotransferase (ALT) and serum albumin (ALB) to those with PBS (**Fig. S7**), confirming that these polymersomal doxorubicin induces insignificant hepatotoxicity.

## 4. Conclusions

We have demonstrated here that cNGQ-PS-Dox is superior to clinically used Lipo-Dox in both subcutaneous and orthotopic A549 human lung cancer models in nude mice. PS-Dox presents several unique benefits over Lipo-Dox, which includes superb control over drug release (*i.e.* low drug leakage under physiological condition and fast drug release inside the tumor cells), unprecedented tolerability and low

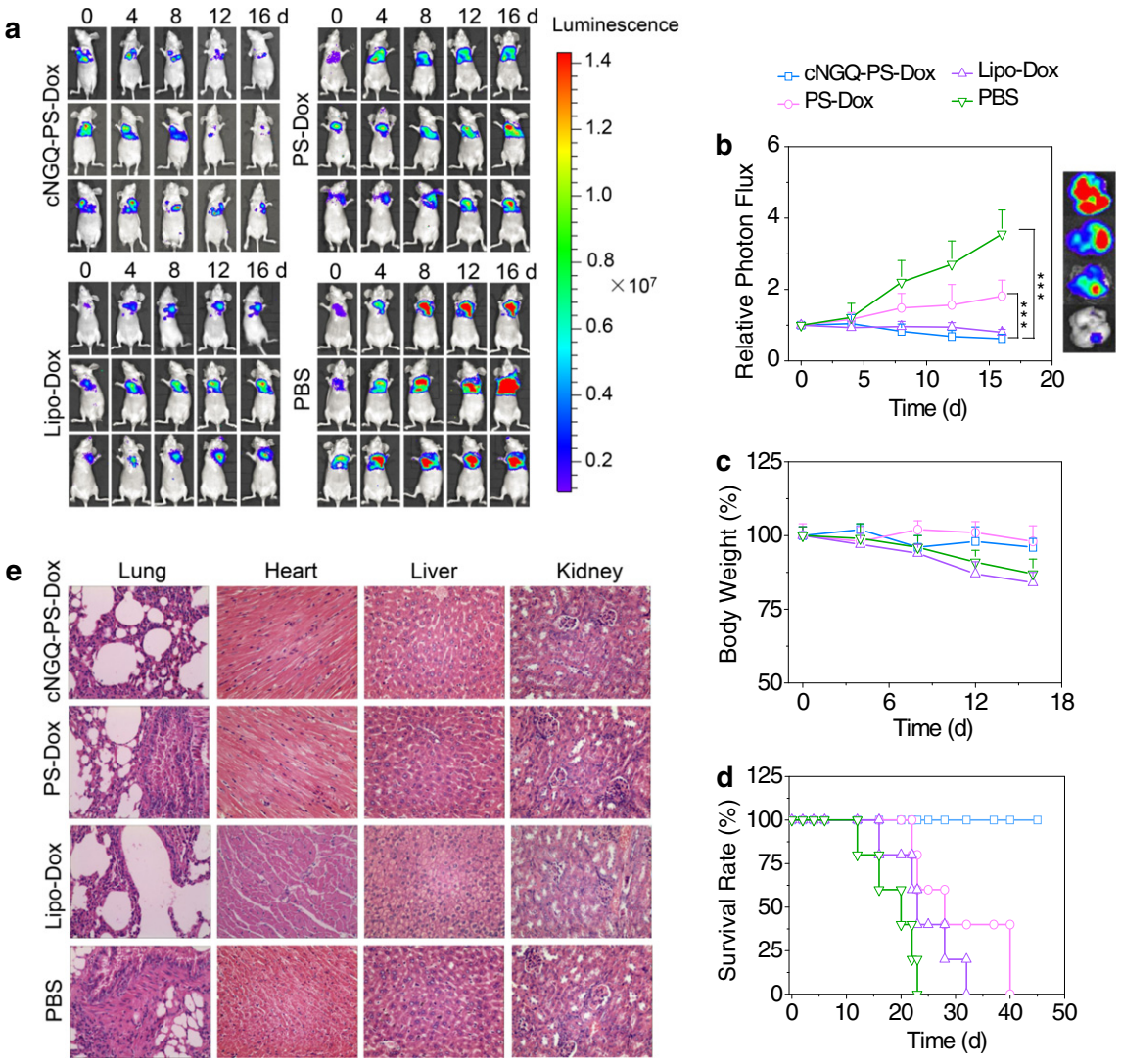


**Fig. 5.** *In vivo* antitumor performance in orthotopic A549-Luc human lung tumor-bearing nude mice. (a) Bioluminescence images of mice treated with cNGQ-PS-Dox, PS-Dox, Lipo-Dox and PBS, respectively. The drug was given on day 0, 4, 8, and 12 (dosage: 7.5 mg DOX·HCl equiv./kg); (b) Average A549-Luc luminescence levels of mice following different treatments. The photos are luminescence images of lung excised on day 16 ($n = 5$, student's test, $^{***}p < 0.001$); (c) Body weight changes of mice in different groups within 16 d; (d) Survival rates of mice in different groups within 45 days; (e) Histological analyses of H&E stained sections of lung, heart, liver and kidney excised from mice following 16 d treatment. The images were obtained under Olympus BX41 microscope using a 40× objective.

systemic toxicity, outstanding tumor selectivity and accumulation, and straightforward fabrication. It should further be noted that PS-Dox provides not only a highly robust but also an extremely versatile nanoplatform that is amenable to facile surface engineering with distinct targeting ligands for various malignancies. This study provides a proof-of-concept that robust, bioresponsive and tumor-homing PS-Dox is a better substitute for Doxil and Caelyx.

## Acknowledgements

This work is supported by research grants from the National Natural Science Foundation of China (NSFC 51273139, 51473111, 51561135010, 51225302), the major project of Jiangsu Province University Natural Science (14KJA150008), Ph.D. Programs Foundation of Ministry of Education of China (20133201110005), Jiangsu Higher Education Excellent Science and Technology Innovation Team Program. Z.Z. thanks the Friedrich Wilhelm Bessel Research Award from the Alexander von Humboldt Foundation.

## Appendix A. Supplementary data

Supplementary data to this article can be found online at http://dx.doi.org/10.1016/j.jconrel.2016.08.022.

## References

[1] D. Peer, J.M. Karp, S. Hong, O.C. Farokhzad, R. Margalit, R. Langer, Nanocarriers as an emerging platform for cancer therapy, Nat. Nanotechnol. 2 (2007) 751–760.
[2] P.T. Hammond, Shooting for the moon: nanoscale approaches to cancer, ACS Nano 10 (2016) 1711–1713.
[3] V.P. Torchilin, Multifunctional, stimuli-sensitive nanoparticulate systems for drug delivery, Nat. Rev. Drug Discov. 13 (2014) 813–827.
[4] R. Cheng, F. Meng, C. Deng, H.-A. Klok, Z. Zhong, Dual and multi-stimuli responsive polymeric nanoparticles for programmed site-specific drug delivery, Biomaterials 34 (2013) 3647–3657.
[5] Y.C. Barenholz, Doxil®-the first FDA-approved nano-drug: lessons learned, J. Control. Release 160 (2012) 117–134.
[6] T.M. Allen, P.R. Cullis, Liposomal drug delivery systems: from concept to clinical applications, Adv. Drug Deliv. Rev. 65 (2013) 36–48.

[7] O. Tacar, P. Sriamornsak, C.R. Dass, Doxorubicin: an update on anticancer molecular action, toxicity and novel drug delivery systems, J. Pharm. Pharmacol. 65 (2013) 157–170.
[8] A. Wicki, D. Witzigmann, V. Balasubramanian, J. Huwyler, Nanomedicine in cancer therapy: challenges, opportunities, and clinical applications, J. Control. Release 200 (2015) 138–157.
[9] V.J. Venditto, F.C. Szoka, Cancer nanomedicines: so many papers and so few drugs! Adv. Drug Deliv. Rev. 65 (2013) 80–88.
[10] R.K. Jain, T. Stylianopoulos, Delivering nanomedicine to solid tumors, Nat. Rev. Clin. Oncol. 7 (2010) 653–664.
[11] H. Cabral, K. Kataoka, Progress of drug-loaded polymeric micelles into clinical studies, J. Control. Release 190 (2014) 465–476.
[12] Y. Min, J.M. Caster, M.J. Eblan, A.Z. Wang, Clinical translation of nanomedicine, Chem. Rev. 115 (2015) 11147–11190.
[13] D.E. Discher, A. Eisenberg, Polymer vesicles, Science 297 (2002) 967–973.
[14] J. Gaitzsch, D. Appelhans, L. Wang, G. Battaglia, B. Voit, Synthetic bio-nanoreactor: mechanical and chemical control of polymersome membrane permeability, Angew. Chem. Int. Ed. 51 (2012) 4448–4451.
[15] K.K. Upadhyay, A.N. Bhatt, A.K. Mishra, B.S. Dwarakanath, S. Jain, C. Schatz, J.-F. Le Meins, A. Farooque, G. Chandraiah, A.K. Jain, The intracellular drug delivery and anti tumor activity of doxorubicin loaded poly (γ-benzyl l-glutamate)-b-hyaluronan polymersomes, Biomaterials 31 (2010) 2882–2892.
[16] D.E. Discher, V. Ortiz, G. Srinivas, M.L. Klein, Y. Kim, D. Christian, S. Cai, P. Photos, F. Ahmed, Emerging applications of polymersomes in delivery: from molecular dynamics to shrinkage of tumors, Prog. Polym. Sci. 32 (2007) 838–857.
[17] C. LoPresti, H. Lomas, M. Massignani, T. Smart, G. Battaglia, Polymersomes: nature inspired nanometer sized compartments, J. Mater. Chem. 19 (2009) 3576–3590.
[18] L. Guan, L. Rizzello, G. Battaglia, Polymersomes and their applications in cancer delivery and therapy, Nanomedicine 10 (2015) 2757–2780.
[19] F. Meng, Z. Zhong, J. Feijen, Stimuli-responsive polymersomes for programmed drug delivery, Biomacromolecules 10 (2009) 197–209.
[20] J.S. Lee, J. Feijen, Polymersomes for drug delivery: design, formation and characterization, J. Control. Release 161 (2012) 473–483.
[21] E. Mabrouk, D. Cuvelier, F. Brochard-Wyart, P. Nassoy, M.-H. Li, Bursting of sensitive polymersomes induced by curling, Proc. Natl. Acad. Sci. U. S. A. 106 (2009) 7294–7298.
[22] L. Zhao, N. Li, K. Wang, C. Shi, L. Zhang, Y. Luan, A review of polypeptide-based polymersomes, Biomaterials 35 (2014) 1284–1301.
[23] J.D. Robertson, G. Yealland, M. Avila-Olias, L. Chierico, O. Bandmann, S.A. Renshaw, G. Battaglia, pH-sensitive tubular polymersomes: formation and applications in cellular delivery, ACS Nano 8 (2014) 4650–4661.
[24] Y. Du, W. Chen, M. Zheng, F. Meng, Z. Zhong, pH-sensitive degradable chimaeric polymersomes for the intracellular release of doxorubicin hydrochloride, Biomaterials 33 (2012) 7291–7299.
[25] H. Sun, F. Meng, R. Cheng, C. Deng, Z. Zhong, Reduction and pH dual-bioresponsive crosslinked polymersomes for efficient intracellular delivery of proteins and potent induction of cancer cell apoptosis, Acta Biomater. 10 (2014) 2159–2168.
[26] T. Thambi, V. Deepagan, H. Ko, D.S. Lee, J.H. Park, Bioreducible polymersomes for intracellular dual-drug delivery, J. Mater. Chem. 22 (2012) 22028–22036.
[27] F. Liu, V. Kozlovskaya, S. Medipelli, B. Xue, F. Ahmad, M. Saeed, D. Cropek, E. Kharlampieva, Temperature-sensitive polymersomes for controlled delivery of anticancer drugs, Chem. Mater. 27 (2015) 7945–7956.
[28] C.-Y. Chen, T.H. Kim, W.-C. Wu, C.-M. Huang, H. Wei, C.W. Mount, Y. Tian, S.-H. Jang, S.H. Pun, A.K.-Y. Jen, pH-dependent, thermosensitive polymeric nanocarriers for drug delivery to solid tumors, Biomaterials 34 (2013) 4501–4509.
[29] G. Liu, X. Wang, J. Hu, G. Zhang, S. Liu, Self-immolative polymersomes for high-efficiency triggered release and programmed enzymatic reactions, J. Am. Chem. Soc. 136 (2014) 7492–7497.
[30] J. Thévenot, H. Oliveira, O. Sandre, S. Lecommandoux, Magnetic responsive polymer composite materials, Chem. Soc. Rev. 42 (2013) 7099–7116.
[31] J.V. Georgieva, R.P. Brinkhuis, K. Stojanov, C.A. Weijers, H. Zuilhof, F.P. Rutjes, D. Hoekstra, J. van Hest, I.S. Zuhorn, Peptide-mediated blood-brain barrier transport of polymersomes, Angew. Chem. Int. Ed. 51 (2012) 8339–8342.
[32] H. Gao, S. Zhang, S. Cao, Z. Yang, Z. Pang, X. Jiang, Angiopep-2 and activatable cell-penetrating peptide dual-functionalized nanoparticles for systemic glioma-targeting delivery, Mol. Pharm. 11 (2014) 2755–2763.
[33] L. Pourtau, H. Oliveira, J. Thevenot, Y. Wan, A.R. Brisson, O. Sandre, S. Miraux, E. Thiaudiere, S. Lecommandoux, Antibody-functionalized magnetic polymersomes: in vivo targeting and imaging of bone metastases using high resolution MRI, Adv. Healthcare Mater. 2 (2013) 1420–1424.
[34] M.A. Yassin, D. Appelhans, R. Wiedemuth, P. Formanek, S. Boye, A. Lederer, A. Temme, B. Voit, Overcoming concealment effects of targeting moieties in the PEG corona: controlled permeable polymersomes decorated with folate-antennae for selective targeting of tumor cells, Small 11 (2015) 1580–1591.
[35] F. Dosio, S. Arpicco, B. Stella, E. Fattal, Hyaluronic acid for anticancer drug and nucleic acid delivery, Adv. Drug Deliv. Rev. 97 (2015) 204–236.
[36] X. Li, W. Yang, Y. Zou, F. Meng, C. Deng, Z. Zhong, Efficacious delivery of protein drugs to prostate cancer cells by PSMA-targeted pH-responsive chimaeric polymersomes, J. Control. Release 220 (2015) 704–714.
[37] X. Wang, G. Liu, J. Hu, G. Zhang, S. Liu, Concurrent block copolymer polymersome stabilization and bilayer permeabilization by stimuli-regulated "traceless" crosslinking, Angew. Chem. Int. Ed. 53 (2014) 3138–3142.
[38] R. Tamate, T. Ueki, R. Yoshida, Self-beating artificial cells: design of cross-linked polymersomes showing self-oscillating motion, Adv. Mater. 27 (2015) 837–842.
[39] S. Mura, J. Nicolas, P. Couvreur, Stimuli-responsive nanocarriers for drug delivery, Nat. Mater. 12 (2013) 991–1003.
[40] A.S. Hoffman, Stimuli-responsive polymers: biomedical applications and challenges for clinical translation, Adv. Drug Deliv. Rev. 65 (2013) 10–16.
[41] K. Raemdonck, S.C. De Smedt, Lessons in simplicity that should shape the future of drug delivery, Nat. Biotechnol. 33 (2015) 1026–1027.
[42] Z. Cheng, A. Al Zaki, J.Z. Hui, V.R. Muzykantov, A. Tsourkas, Multifunctional nanoparticles: cost versus benefit of adding targeting and imaging capabilities, Science 338 (2012) 903–910.
[43] M. Barz, Complexity and simplification in the development of nanomedicines, Nanomedicine 10 (2015) 3093–3097.
[44] Y. Zou, Y. Fang, H. Meng, F. Meng, J. Zhang, C. Deng, Z. Zhong, Self-crosslinkable and intracellularly decrosslinkable biodegradable micellar nanoparticles: a robust, simple and multifunctional nanoplatform for high-efficiency targeted cancer chemotherapy, J. Control. Release (2016), http://dx.doi.org/10.1016/j.jconrel.2016.05.060.
[45] L.S. Nair, C.T. Laurencin, Biodegradable polymers as biomaterials, Prog. Polym. Sci. 32 (2007) 762–798.
[46] A. Maczurek, K. Hager, M. Kenklies, M. Sharman, R. Martins, J. Engel, D.A. Carlson, G. Münch, Lipoic acid as an anti-inflammatory and neuroprotective treatment for Alzheimer's disease, Adv. Drug Deliv. Rev. 60 (2008) 1463–1470.
[47] Y.L. Li, L. Zhu, Z. Liu, R. Cheng, F. Meng, J.H. Cui, S.J. Ji, Z. Zhong, Reversibly stabilized multifunctional dextran nanoparticles efficiently deliver doxorubicin into the nuclei of cancer cells, Angew. Chem. Int. Ed. 48 (2009) 9914–9918.
[48] D. Lau, L. Guo, R. Liu, J. Marik, K. Lam, Peptide ligands targeting integrin alpha 3 beta 1 in non-small cell lung cancer, Lung Cancer 52 (2006) 291–297.
[49] X. Li, D.J. Hirsh, D. Cabral-Lilly, A. Zirkel, S.M. Gruner, A.S. Janoff, W.R. Perkins, Doxorubicin physical state in solution and inside liposomes loaded via a pH gradient, Biochim. Biophys. Acta Biomembr. 1415 (1998) 23–40.
[50] S.C. Owen, D.P. Chan, M.S. Shoichet, Polymeric micelle stability, Nano Today 7 (2012) 53–65.
[51] T. Lammers, F. Kiessling, W.E. Hennink, G. Storm, Drug targeting to tumors: principles, pitfalls and (pre-) clinical progress, J. Control. Release 161 (2012) 175–187.
[52] S.-D. Li, L. Huang, Pharmacokinetics and biodistribution of nanoparticles, Mol. Pharm. 5 (2008) 496–504.
[53] R.L. Pierce, Translational nanomedicine-through the therapeutic window, Nanomedicine 10 (2015) 3249–3260.